9th ECCOMAS Thematic Conference on the Mechanical Response of Composites
COMPOSITES 2023
G. Catalanotti, H. Petterman and G. Pittaresi (Eds)

A 3D DAMAGE MODEL FOR SIMULATING DAMAGE MODES IN FIBRE METAL LAMINATES

Ibrahim H. Abuzayed[1*], Nanda Wirawan[1], Chao Zhang[2], Jose L. Curiel-Sosa[1]

[*1]Department of Mechanical Engineering, University of Sheffield, Sheffield, UK
[2]School of Mechanical Engineering, Jiangsu University, Zhenjiang, China
[*] ihabuzayed1@sheffield.ac.uk

Keywords: Damage mechanisms, 3D puck, fracture plane, GLARE

Summary: *This paper presents a 3D damage model utilized for studying the failure characteristics of GLARE. The current damage model adopted the 3D forms of Hashin's and Puck's failure criteria for predicting the onset of failure of fibres and matrix in the composite plies. Whilst the damage evolution is modelled based on the dissipation of fracture energy. In addition, a ductile damage model was employed to study the failure of metal layers and the delamination was assessed via a cohesive interface model. The current damage model was adopted to predict the failure modes and the blunt notch strength of GLARE; where various failure modes were observed, such as Fibre breakage, matrix cracking, delamination and plastic damage of aluminium layers. The model showed strong agreement with experimental results.*

1 INTRODUCTION

Fibre metal laminates are hybrid materials consisting of metal and fibre composite layers stacked in a certain layup sequence. The integration of both constituents was intended to improve the mechanical behaviour of the resultant material. FMLs have shown evident improvements in fatigue resistance, strength as well as weight reduction compared to conventional materials [1]. Consequently, this provides a significant advantage in certain aerospace applications such as wing structures, fuselage and ballistic protection [1].

Aircraft structures contain unavoidable holes, therefore, it is essential to understand the behaviour of notched FML structures. The blunt notch strength of FMLs have been widely investigated experimentally for different notch shapes and sizes [2, 6]. Additionally, the literature showed some numerical simulations, mainly 2D models, for notched FMLs such as [8, 6, 7, 4]. However, most of the published work does not consider the initiation and propagation of damage in the out-of-plane direction. In addition, crack propagation and failure sequence of the layers are not well investigated numerically in FMLs containing voids.

This paper presents a comprehensive damage model for predicting damage modes in FML's constituents. In the current damage model, the initiation and evolution of damage as well as crack propagation were predicted across FML layers. The model was implemented in the Explicit solver ABAQUS through a user defined subroutine (VUMAT).

2 OPEN HOLE TENSILE TEST OF GLARE

The open hole tensile test of glass laminate aluminium reinforced epoxy (GLARE) is simulated based on the specifications of an experimental test done by De Vries [2]. A coupon specimen with a single hole is used in the experimental test, the dimensions of the specimen are shown in Figure 1. The specimen consists of GLARE 3 3/2-0.3, which has three aluminium layers each with a thickness of 0.3 mm and two glass fibre prepreg layers with [0°,90°] fibre orientation, where the thickness of the laminate is 0.25 mm. A schematic diagram describing the cross-section of the specimen is shown in Figure 2. In the FE model, the specimen is fixed in all directions at the clamping end, while the loading end is allowed to deform only in the load direction. The load is applied at a reference point located at the middle of the loading edge, where all nodes at the loading edge are coupled to a reference point, which simplifies data collection in the post-processing stage.

As this research is aimed to study the fracture of FMLs, a full model of the specimen should be modelled to predict the failure mechanisms and cracks at failure. The full specimen is considered in this study, therefore all the layers were modelled with the actual dimensions of the test specimen. The layers were combined together as shown in Figure 2, where a cohesive interaction was defined at the interface of the layers. All layers were assigned the 3D 8-node linear brick elements with reduced integration (C3D8R) available in ABAQUS.

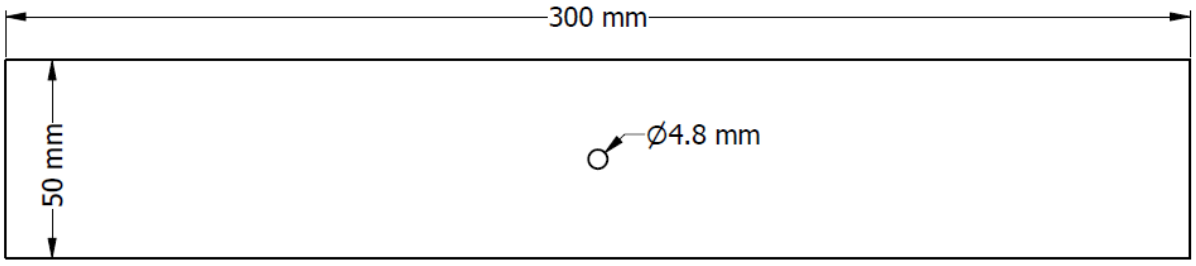

Figure 1: GLARE-3 specimen geometry

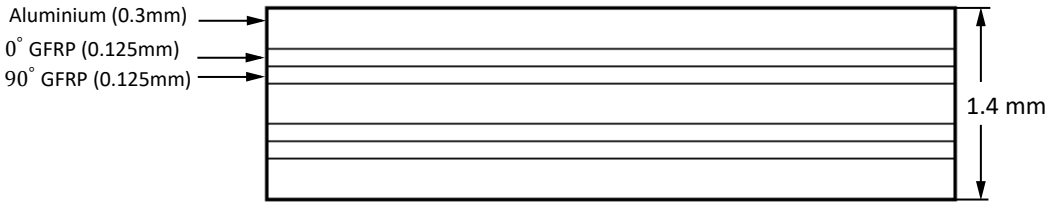

Figure 2: GLARE-3 cross-sectional view

2.1 Material properties of GLARE

The aluminium layers in GLARE were assigned the elastic properties of aluminium 2024-T3 listed in Table 1. The plasticity of aluminium was considered with isotropic

hardening data available in [8]. Whereas the behaviour of Glass fibre layers is assumed to be transversely isotropic; the elastic material properties and strength values of glass fibre are listed in Tables 2 and 3. The damage model implemented for glass fibre layers depends on fracture energies defined in Table 4.

Table 1: Mechanical properties of aluminium 2024-T3 [8, 14]

$\rho(Kg/m^3)$	ν	E(GPa)	Yield strength (MPa)	Fracture energy (J/m^2)
2770	0.33	72.2	300	10.2

Table 2: Orthotropic elastic properties of glass fibre prepreg [8]

E_1(GPa)	$E_2 = E_3$(GPa)	$G_{12} = G_{13}$(GPa)	G_{23}(MPa)	$\nu_{12} = \nu_{13}$
55.0	9.5	5.5	3.0	0.33

Table 3: Orthotropic strength of glass fibre prepreg [8]

X^T(MPa)	X^C(MPa)	Y^T(MPa)	Y^C(MPa)	S^L(MPa)
2500	2000	50	150	50

Table 4: Fracture energies of glass fibre prepreg [10]

G_{ft}(N/mm)	G_{fc}(N/mm)	G_{mt}(N/mm)	G_{mc}(N/mm)
32	20	4.5	4.5

3 PROGRESSIVE DAMAGE OF FMLS

3.1 Damage model of glass fibre

The current model incorporates several criteria, interface model and damage evolution law with the aim of replicating the complex failure mechanisms occurring in FMLs under certain loading conditions and configurations. Hashin's and Puck's failure criteria were used for predicting the damage initiation of fibre and matrix in glass fibre layers. The progression of damage is modeled with a damage evolution law proposed by I. Lapczyk and J. Hurtado [8]. This formulation was implemented in the explicit FE solver ABAQUS through a user defined subroutine (VUMAT). As the available damage model in ABAQUS does not support damage initiation and propagation in the out of plane direction.

3.1.1 Fibre failure criteria

Hashin's fibre failure criterion was chosen to assess the damage initiation in fibres [5]. The criterion considers two damage modes: fibre tension and compression, which are expressed based on the strength along fibre direction and the in- and out- of plane shear strengths as shown below.

Fibre tension ($\hat{\sigma}_{11} \geq 0$)

$$F_{ft} = \left(\frac{\hat{\sigma}_{11}}{X^T}\right)^2 + \left(\frac{\hat{\sigma}_{12}}{S^L}\right)^2 + \left(\frac{\hat{\sigma}_{13}}{S^L}\right)^2 = 1 \tag{1}$$

Fibre compression ($\hat{\sigma}_{11} < 0$)

$$F_{fc} = \left(\frac{\hat{\sigma}_{11}}{X^C}\right)^2 = 1 \tag{2}$$

3.1.2 Matrix failure criteria

Puck's inter fibre fracture (IFF) criterion was adopted in the current model to assess the damage initiation in the matrix (epoxy). The criterion was developed based on the brittle behaviour of composites while assuming transversely isotropic behaviour [3]. IFF is based on three stress components ($\sigma_n, \tau_{nt}, \tau_{nl}$) acting on a plane parallel to fibre direction as shown in Figure 3. Therefore, the first step for implementing IFF starts with the derivation of the action plane stresses from the stresses applied at normal directions (X_1, X_2, X_3). Then the fracture resistances are calculated at the action plane which are: ($R^{At}_{\parallel\perp}, R^A_{\perp\perp}, R^A_{\perp}$), where $\perp$ *and* $\parallel$ indicates a direction perpendicular and parallel to fibre's direction respectively, while the subscript (A) represents the action plane. ($R^{At}_{\parallel\perp}$) and ($R^A_{\perp}$) denote the transverse tensile strength and in-plane shear strength respectively, note that those parameters were defined as (Y_T *and* S_L) in Table 3. The third fracture resistance $R^A_{\perp\perp}$ is calculated from equation 3.

$$R^A_{\perp\perp} = \frac{R^c_{\perp}}{2(1 + p^c_{\perp\perp})} \tag{3}$$

Where $R^c_{\perp}$ is the transverse compressive strength and $p^c_{\perp\perp}$ is the inclination parameter which equals 0.25 for glass fibre as suggested by [9].

The final step of implementing IFF involves a numerical search for the fracture angle (θ_{fp}), this is the angle (θ) in Figure 3, which is ranging from -90° to 90°. Various numerical methods for finding (θ_{fp}) are available in the literature such as the search algorithm proposed by [13]. In the current study, (θ_{fp}) was defined as the fracture plane angle at the maximum stress exposure value. Therefore, Equations 4 and 5 were calculated for (θ) ranging from -90° to 90° then the maximum value was saved in damage initiation variable, i.e. $f_{E,IFF+} = maxval(f_{E,IFF+}(\theta))$ and $f_{E,IFF-} = maxval(f_{E,IFF-}(\theta))$. In the subroutine, the stress exposure values were used as activation functions for the damage evolution law.

For $\sigma_n \geq 0$

$$f_{E,IFF+}(\theta) = \sqrt{\left[\left(\frac{1}{R^{At}_{\perp}} - \frac{p^t_{\perp\psi}}{R^A_{\perp\psi}}\right)\bar{\sigma}_n(\theta)\right]^2 + \left(\frac{\bar{\tau}_{nt}(\theta)}{R^A_{\perp\perp}}\right)^2 + \left(\frac{\bar{\tau}_{n1}(\theta)}{R^A_{\parallel\perp}}\right)^2} + \frac{p^t_{|\psi}}{R^A_{\perp\psi}}\bar{\sigma}_n(\theta) \tag{4}$$

For $\sigma_n < 0$

$$f_{E,IFF-}(\theta) = \sqrt{\left(\frac{p^c_{\perp\psi}}{R^A_{\perp\psi}}\bar{\sigma}_n(\theta)\right)^2 + \left(\frac{\bar{\tau}_{nt}(\theta)}{R^A_{\perp\perp}}\right)^2 + \left(\frac{\bar{\tau}_{n1}(\theta)}{R^A_{\parallel\perp}}\right)^2} + \frac{p^t_{|\psi}}{R^A_{\perp\psi}}\bar{\sigma}_n(\theta) \tag{5}$$

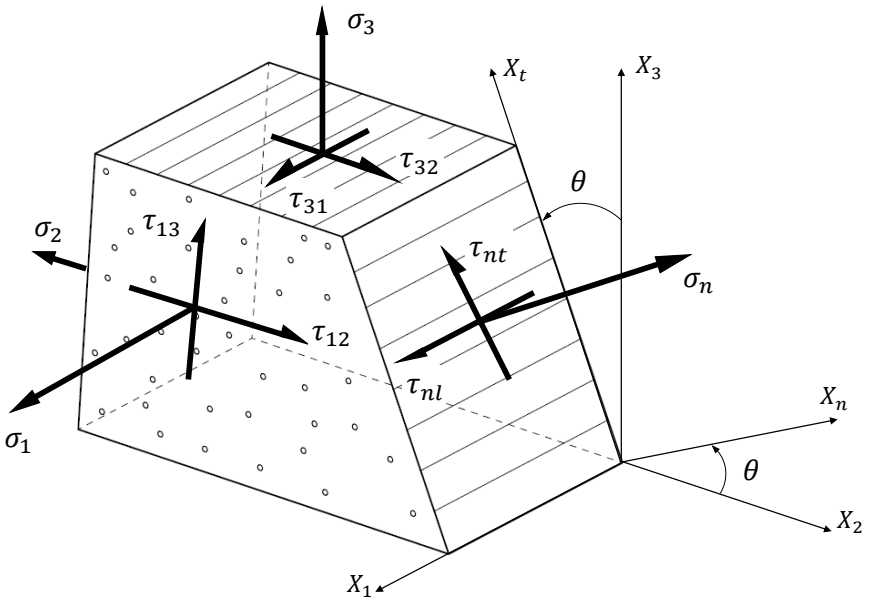

Figure 3: Definition of stresses $(\sigma_n, \tau_{nt}, \tau_{n1})$ on fibre parallel plane

3.1.3 Damage evolution

Once the damage is initiated at a material point, the stiffness matrix coefficients are degraded based on the damage evolution law. The evolution law in the current model is based on the energy dissipated during damage where it is controlled by the equivalent displacements and stresses [8]. This formulation was proposed by I. Lapczyk and J. Hurtado [8] for 2D fibre composites and was implemented in an implicit solver. In this study, Lapcyk's evolution law was extended to account for 3D stresses in order to ensure compatibility with the initiation criteria presented in the previous sections.

$$d_I = \frac{\delta^f_{I,eq}(\delta_{I,eq} - \delta^0_{I,eq})}{\delta_{I,eq}(\delta^f_{I,eq} - \delta^0_{I,eq})}; \qquad I \in \{ft, fc, mt, mc\} \tag{6}$$

The damage variables were calculated for each damage mode using equation 6, where $\delta^0_{I,eq}$ *and* $\delta^f_{I,eq}$ are the equivalent displacements at damage initiation and at full failure respectively. In equation 6, the initial and final equivalent displacements were calculated using equations 7 and 8, F_I indicates the damage initiation variable for $I \in \{ft, fc, mt, mc\}$.

While $\delta_{I,eq}$ and $\sigma_{I,eq}$ indicate the current equivalent displacement and stress, which were calculated using the equations listed in Table 5.

$$\delta^0_{I,eq} = \frac{\delta_{I,eq}}{\sqrt{F_I}} \tag{7}$$

$$\delta^f_{I,eq} = \frac{2G_{I,c}}{\sigma_{I,eq}} \tag{8}$$

$$\sigma^0_{I,eq} = \frac{\sigma_{I,eq}}{\sqrt{F_I}} \tag{9}$$

Table 5: Equivalent displacements and stresses

Damage mode	$\delta_{I,eq}$	$\sigma_{I,eq}$
Fibre traction ($\sigma_{11} \geq 0$)	$L_c\sqrt{\langle\varepsilon_{11}\rangle^2 + \varepsilon_{12}^2 + \varepsilon_{13}^2}$	$\frac{L_c(\langle\sigma_{11}\rangle\langle\varepsilon_{11}\rangle+\sigma_{12}\varepsilon_{12}+\sigma_{13}\varepsilon_{13})}{\delta_{eq,ft}}$
Fibre compression ($\sigma_{11} < 0$)	$L_c\langle-\varepsilon_{11}\rangle$	$\frac{L_c(\langle-\sigma_{11}\rangle\langle-\varepsilon_{11}\rangle)}{\delta_{eq,fc}}$
Matrix traction ($\sigma_{22} \geq 0$)	$L_c\sqrt{\langle\varepsilon_{22}\rangle^2 + \varepsilon_{12}^2 + \varepsilon_{23}^2}$	$\frac{L_c(\langle\sigma_{22}\rangle\langle\varepsilon_{22}\rangle+\sigma_{12}\varepsilon_{12}+\sigma_{23}\varepsilon_{23})}{\delta_{eq,mt2}}$
Matrix compression ($\sigma_{22} < 0$)	$L_c\sqrt{\langle-\varepsilon_{22}\rangle^2 + \varepsilon_{12}^2 + \varepsilon_{23}^2}$	$\frac{L_c(\langle-\sigma_{22}\rangle\langle-\varepsilon_{22}\rangle+\sigma_{12}\varepsilon_{12}+\sigma_{23}\varepsilon_{23})}{\delta_{eq,mc2}}$
Matrix traction ($\sigma_{33} \geq 0$)	$L_c\sqrt{\langle\varepsilon_{33}\rangle^2 + \varepsilon_{13}^2 + \varepsilon_{23}^2}$	$\frac{L_c(\langle\sigma_{33}\rangle\langle\varepsilon_{33}\rangle+\sigma_{13}\varepsilon_{13}+\sigma_{23}\varepsilon_{23})}{\delta_{eq,mt3}}$
Matrix compression ($\sigma_{33} < 0$)	$L_c\sqrt{\langle-\varepsilon_{33}\rangle^2 + \varepsilon_{13}^2 + \varepsilon_{23}^2}$	$\frac{L_c(\langle-\sigma_{33}\rangle\langle-\varepsilon_{33}\rangle+\sigma_{13}\varepsilon_{13}+\sigma_{23}\varepsilon_{23})}{\delta_{eq,mc3}}$

3.1.4 Element deletion

Finally, the failed elements were deleted from the model to simulate the crack propagation phenomena in the specimen. The element deletion criterion used in this model is based on the damage threshold and the change of volume in a certain element; this was accomplished by computing the determinant of the deformation gradient ($det(F)$) which is defined as the ratio of the deformed volume to the undeformed volume ($\frac{V}{V_0}$) [12]. The criterion is defined as follows:

$$\begin{cases} d_{ft} \geq 0.99 \; and \; det(F) \geq 1.2 \\ \; OR \\ d_{mt} \geq 0.99 \; and \; det(F) \geq 1.2 \end{cases} \tag{10}$$

3.2 Ductile materials failure criterion

The damage in aluminium layers was assessed based on the ductile damage model available in ABAQUS. This model depends on the equivalent plastic strain ($\bar{\varepsilon}^{pl}_D$) at a material point as shown in equation 11 [11]. The criterion is satisfied when the state variable (ω_D) approaches 1.

$$\omega_D = \int \frac{d\bar{\varepsilon}^{pl}}{\bar{\varepsilon}^{pl}_D(\eta, \dot{\bar{\varepsilon}}^{pl})} = 1 \tag{11}$$

Once the damage accumulates in a material point and reaches the onset of damage, the element stiffness degrades based on a linear damage evolution law. Which was defined by the fracture energy, described in Table 1, dissipated during the damage process [11].

3.3 Interface damage model

The consideration of inter-laminar failure was important to model the comprehensive damage process in FMLs. In the current model, a mixed-mode traction separation model was embedded at the interface across FML layers. The benzeggagah-kenane (BK) damage model was applied as a damage evolution for the cohesive interface, where the parameters used in the definition of the cohesive model are defined in Table 6.

Table 6: Cohesive model parameters

E(GPa)			(MPa)			G_c(N/mm)		
E_{nn}	E_{ss}	E_{tt}	t^0_n	t^0_t	t^0_t	$G_{\|c}$	$G_{\|\|c}$	$G_{\|\|\|c}$
2	0.75	0.75	65	38	38	2	3	3

4 RESULTS AND DISCUSSION

The damage mechanisms captured during the open hole tensile test of GLARE involved fibre breakage, matrix cracking, delamination and plastic damage of aluminium layers. In the following sections, the critical failure modes will be analysed in each constituent of GLARE.

4.1 Progressive damage in glass fibre layers

In the 90° glass fibre layers, matrix cracking tends to be the most critical failure mode, while no evident fibre failure was observed in these layers. Matrix cracking in tension was the first failure mode that appeared in the specimen. Figure 4 illustrates the matrix tension damage variable (d_{mt}) in three increments, where it indicates matrix cracking propagation. The damage accumulated around notch edges at an early increment (Figure 4-a), then cracks propagate in a direction perpendicular to the loading axis as shown in Figures 4-b & c. Indeed, a butterfly shape is exhibited through the propagation of matrix damage.

Two failure modes were observed in the 0° glass fibre layers: fibre breakage and matrix cracking as shown in Figure-5 & 6. The matrix damage was observed before the fibre tension damage in these layers. However, both damages accumulated around the notch and propagate initially in the fibre direction. Then additional cracks were formed in a diagonal direction as shown in Figure-5-b & 6-b.

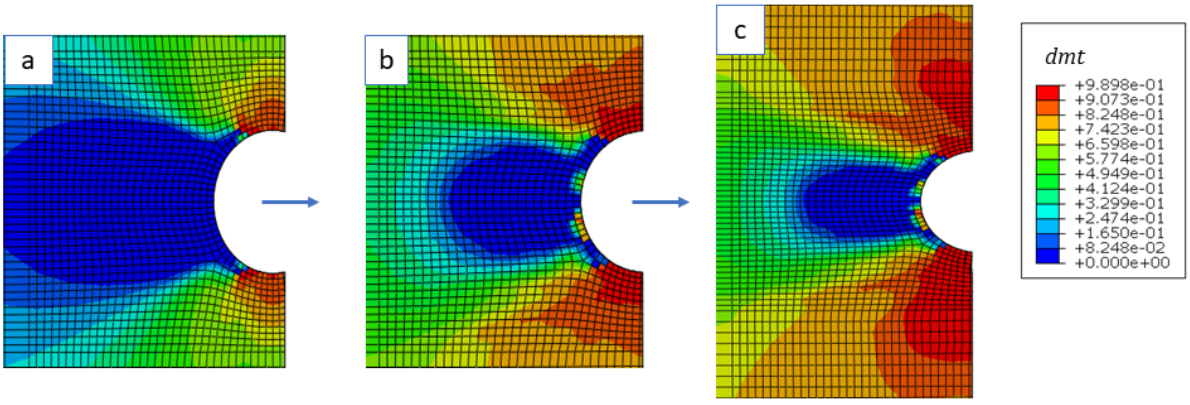

Figure 4: Matrix damage in tension in the 90° glass fibre layers

Prior to full failure cracks appeared in the regions above and below the notch, as illustrated in Figure-5-c & 6-c. The change of damage direction occurred due to the formation of cracks in the 90° layers in the perpendicular direction.

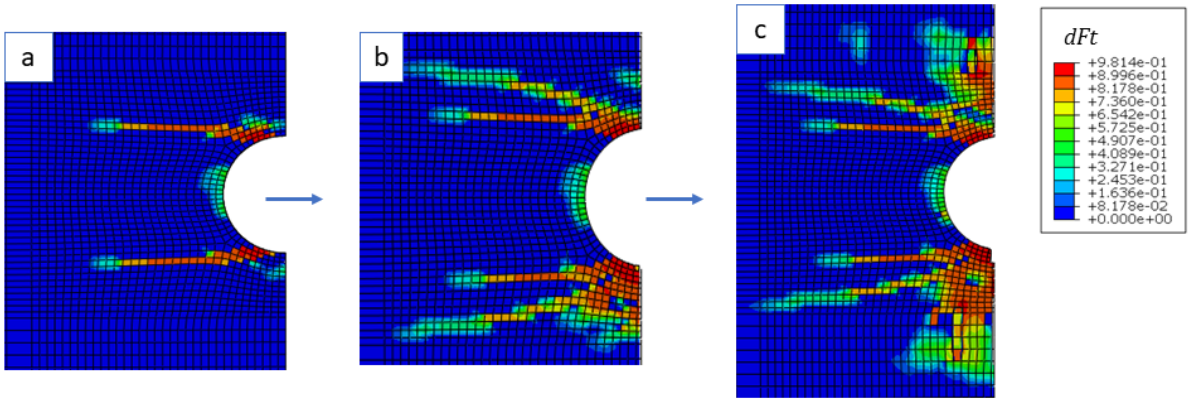

Figure 5: fibre damage in tension in the 0° glass fibre layers

4.2 Progressive damage in aluminium layers

Aluminium layers reached the yield point at an early stage, whilst the full failure was achieved after the failure of glass fibre layers. The contour plots of von-mises stress and ductile damage (DUCTCRT) are illustrated in Figures-7-a & b respectively, both figures show the highest values in the perpendicular direction. Furthermore, necking was visible at the edges of the specimen after the failure of composite layers, as illustrated in Figure 8-b.

Delamination was evident mostly at the interface of aluminium and 0° glass fibre layers which agreed with the predictions of I. Lapczyk and J. Hurtado [8]. The contact stress

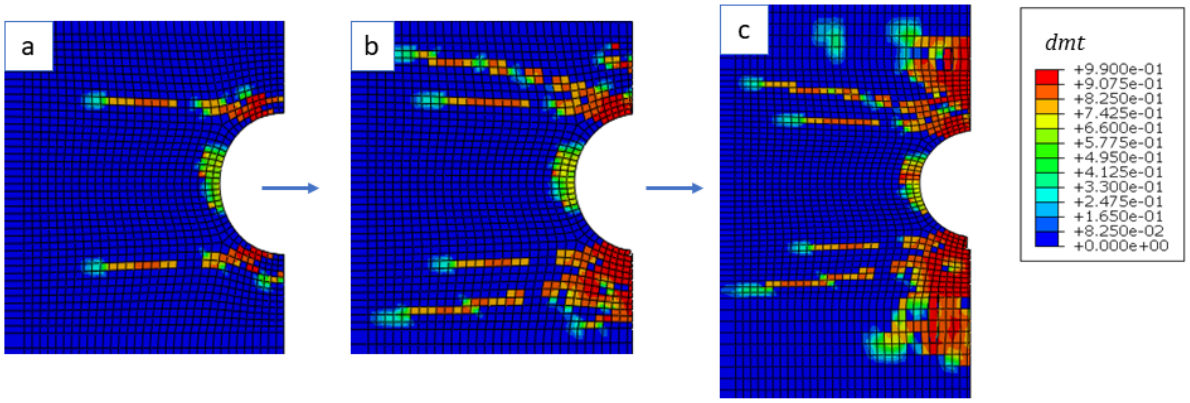

Figure 6: Matrix damage in tension in the 0° glass fibre layers

damage initiation variable (CSMAXSCRT) was satisfied around the notch before the full failure, which indicates separation of layers as illustrated in Figure 7-c.

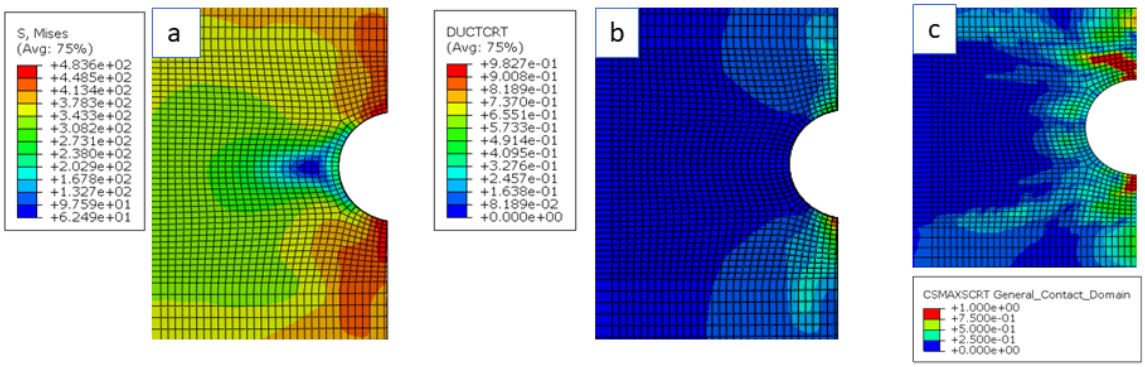

Figure 7: (a) Von-Mises stress (b) Ductile damage (c) CSMAXSCRT

4.3 The failure sequence in GLARE

The failure sequence of open hole GLARE laminates subjected to tensile loading started with yielding of aluminium layers followed by matrix cracking in the 90°,0° layers, fibre breakage in the 0° layers and finally fracture of the aluminium layers. It was evident that glass fibre layers were cracked before aluminium layers as noted in Figure 8b. This could be explained by the fact that aluminium 2024-T3 holds more strain compared to glass fibre due to its ductile behaviour. However, once the crack propagated in the glass fibre layers, the aluminium was incapable of resisting the stress and failed instantaneously. Figure-8-c shows the specimen after full failure. The final crack is perpendicular to the loading direction which indicates a brittle failure, this correlates well with experimental observations in [7] for an FML with similar fibre orientations.

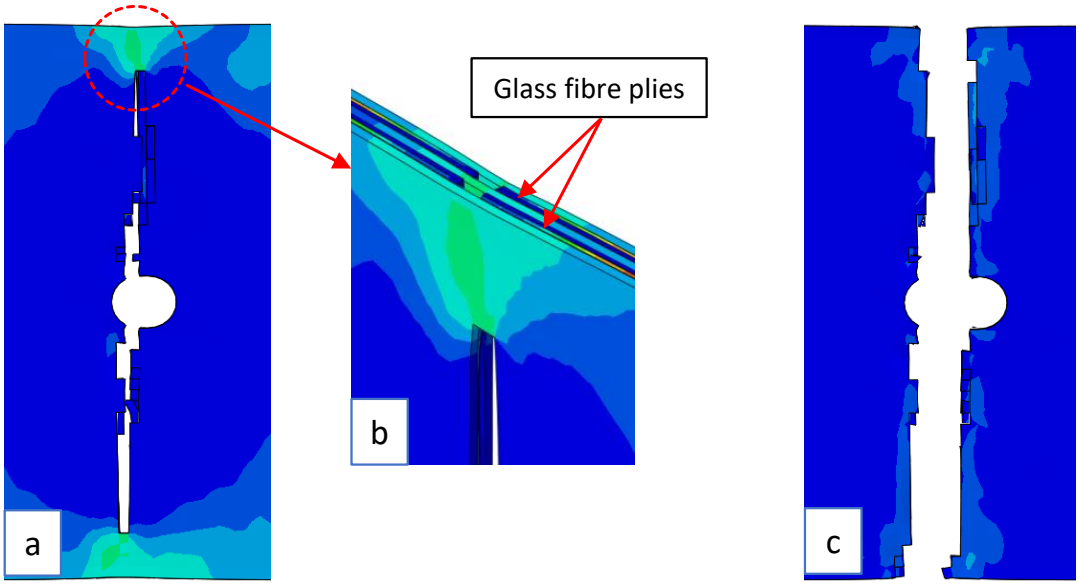

Figure 8: Crack propagation in GLARE specimen

5 STRESS-STRAIN RELATIONSHIP

The stress-strain curve of the open-hole tensile test specimen of GLARE was calculated from force-displacement data obtained from the FE simulation, the curve is illustrated in Figure 9. The blunt notch strength (S_{BN}) was calculated from equation 12, where S_{max} is the maximum stress, W is the total width, D is the diameter and t is the thickness of the specimen.

$$S_{BN} = \frac{S_{max}}{(W - D)t} \tag{12}$$

The overall ultimate tensile strength of the specimen is 441 MPa, this value correlated well with the experimental results by [2], where the error is less than 5%. The stress-strain curve has shown three main regions: an elastic linear curve, a nonlinear curve indicating the yield region of aluminium and a linear curve with a more steep modulus. The Young's modulus is 63 GPa, indicating approximately 5% difference of the predictions outlined in [8].

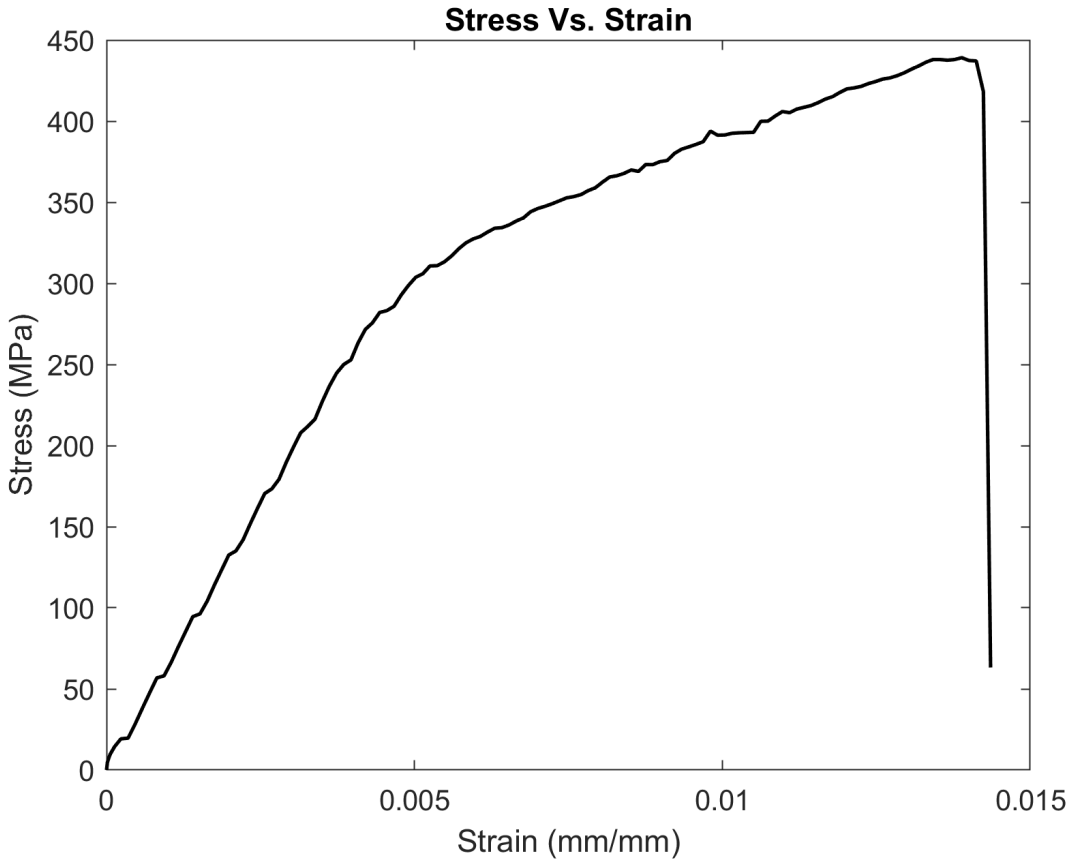

Figure 9: Stress strain curve

6 CONCLUSION

A 3D finite element damage model was developed to investigate the failure mechanisms of FMLs. Puck's fracture plane theory was implemented for predicting the damage threshold in glass fibre plies and the evolution of damage was controlled using the equivalent displacements and stresses in three dimensions. The damage model was used to predict the mechanical behaviour and failure mechanisms of GLARE. The model successfully captured fibre breakage, matrix cracking, delamination and ductile failure in GLARE constituents, as well as the failure sequence and crack direction. In addition, the stress-strain curve of GLARE was predicted where the blunt notch strength correlated well with experimental results.

REFERENCES

[1] Edson Cocchieri Botelho, Rogério Almeida Silva, Luiz Cláudio Pardini, and Mirabel Cerqueira Rezende. A review on the development and properties of continuous fiber/epoxy/aluminum hybrid composites for aircraft structures. *Materials Research*, 9:247–256, 2006.

[2] T.J. De Vries. Blunt and sharp notch behaviour of glare laminates. *Ph.D dissertation*, 2001.

[3] H Matthias Deuschle and Alfred Puck. Application of the puck failure theory for fibre-reinforced composites under three-dimensional stress: Comparison with experimental results. *Journal of Composite Materials*, 47(6-7):827–846, 2013.

[4] Dandan Du, Yubing Hu, Huaguan Li, Cheng Liu, and Jie Tao. Open-hole tensile progressive damage and failure prediction of carbon fiber-reinforced peek–titanium laminates. *Composites Part B: Engineering*, 91:65–74, 2016.

[5] Zvi Hashin. Fatigue failure criteria for unidirectional fiber composites. *Journal of applied mechanics*, 47(4):329–334, 1980.

[6] Wentao He, Changzi Wang, Shuqing Wang, Lu Yao, Linfeng Wang, and De Xie. Characterizing and predicting the tensile mechanical behavior and failure mechanisms of notched fmls—combined with dic and numerical techniques. *Composite Structures*, 254:112893, 2020.

[7] Wentao He, Changzi Wang, Shuqing Wang, Lu Yao, Jun Wu, and De Xie. Tensile mechanical behavior and failure mechanisms of multihole fiber metal laminates—experimental characterization and numerical prediction. *Journal of Reinforced Plastics and Composites*, 39(13-14):499–519, 2020.

[8] Ireneusz Lapczyk and Juan A. Hurtado. Progressive damage modeling in fiber-reinforced materials. *Composites. Part A, Applied science and manufacturing*, 38(11):2333–2341, 2007.

[9] H Matthias Deuschle and Bernd-H Kröplin. Finite element implementation of puck's failure theory for fibre-reinforced composites under three-dimensional stress. *Journal of composite materials*, 46(19-20):2485–2513, 2012.

[10] Seyed Saeid Rahimian Koloor, Atefeh Karimzadeh, Noorfaizal Yidris, Michal Petr, Majid Reza Ayatollahi, and Mohd Nasir Tamin. An energy-based concept for yielding of multidirectional frp composite structures using a mesoscale lamina damage model. *Polymers*, 12(1):157, 2020.

[11] Michael Smith. *ABAQUS/Standard User's Manual, Version 6.9*. Dassault Systèmes Simulia Corp, United States, 2009.

[12] Wei Tan and Brian G Falzon. Modelling the crush behaviour of thermoplastic composites. *Composites Science and Technology*, 134:57–71, 2016.

[13] J Wiegand, N Petrinic, and B Elliott. An algorithm for determination of the fracture angle for the three-dimensional puck matrix failure criterion for ud composites. *Composites Science and Technology*, 68(12):2511–2517, 2008.

[14] Guoqi Zhang, Bing Wang, Li Ma, Jian Xiong, Jinshui Yang, and Linzhi Wu. The residual compressive strength of impact-damaged sandwich structures with pyramidal truss cores. *Composite Structures*, 105:188–198, 2013.